Published in final edited form as:
Nat Neurosci. 2015 December ; 18(12): 1845–1852. doi:10.1038/nn.4161.

Optogenetic Acidification of Synaptic Vesicles and Lysosomes

Benjamin R. Rost[#1,2,9], **Franziska Schneider**[#3,7], **M. Katharina Grauel**[1], **Christian Wozny**[1,4], **Claudia Bentz**[1], **Anja Blessing**[5,6], **Tanja Rosenmund**[1], **Thomas J. Jentsch**[5,6], **Dietmar Schmitz**[1,2], **Peter Hegemann**[3], and **Christian Rosenmund**[1]

[1]Neuroscience Research Center, Charité – Universitätsmedizin Berlin, Berlin, Germany

[2]German Center for Neurodegenerative Diseases (DZNE), Berlin, Germany

[3]Institute of Biology, Experimental Biophysics, Humboldt-Universität zu Berlin, Berlin, Germany

[4]University of Strathclyde, Glasgow, UK

[5]Max-Delbrück-Centrum für Molekulare Medizin (MDC), Berlin, Germany

[6]Leibniz-Institut für Molekulare Pharmakologie (FMP), Berlin, Germany

[7]Current address: National Heart and Lung Institute, Imperial College London, United Kingdom

[#] These authors contributed equally to this work.

Abstract

Acidification is required for the function of many intracellular organelles, but methods to acutely manipulate their intraluminal pH have not been available. Here we present a targeting strategy to selectively express the light-driven proton pump Arch3 on synaptic vesicles. Our new tool, pHoenix, can functionally replace endogenous proton pumps, enabling optogenetic control of vesicular acidification and neurotransmitter accumulation. Under physiological conditions, glutamatergic vesicles are nearly full, as additional vesicle acidification with pHoenix only slightly increased the quantal size. By contrast, we found that incompletely filled vesicles exhibited a lower release probability than full vesicles, suggesting preferential exocytosis of vesicles with high transmitter content. Our subcellular targeting approach can be transferred to other organelles, as demonstrated for a pHoenix variant that allows light-activated acidification of lysosomes.

The release of neurotransmitters from synaptic vesicles is a key element of chemical synaptic transmission. Synaptic vesicle recycling after exo- and endocytosis requires neurotransmitter uptake by specialized vesicular transporter proteins1. The electrochemical driving force for neurotransmitter accumulation is generated by vacuolar-type H^+-ATPases (V-ATPases) that actively transport cytosolic protons into the synaptic vesicle lumen, thereby acidifying the vesicles and generating an inside positive membrane potential2. V-ATPases

[9]Correspondence tobenjamin.rost@dzne.de.

Author contributions:
B.R.R. and F.S. developed the concepts for the pHoenix constructs. F.S. performed the molecular biology. B.R.R., F.S., M.K.G., C.W., C.B., A.B and T.R. performed the experiments and analyzed the data. All authors designed the experiments and discussed the results. B.R.R. and F.S. prepared the manuscript, and all authors contributed to editing the paper.

Europe PMC Funders Author Manuscripts

also acidify other subcellular compartments of the secretory and endocytic pathways such as endosomes, Golgi-derived vesicles and lysosomes, but to a different extent, with lysosomes being the most acidic compartments in a cell (pH < 5)3. The tightly regulated acidification of these organelles is a prerequisite for a plethora of different processes including processing, storage and degradation of proteins, lipids, and polysaccharides3,4. However, elucidating the physiological roles of V-ATPases has remained challenging due to the lack of tools that allow rapid and compartment-specific control of proton accumulation.

The recent advance of optogenetic methods allows for precise manipulation of multiple cellular activities with light. In neuroscience, microbial rhodopsins such as channelrhodopsins and light-activated ion pumps are applied to modulate the neuronal membrane potential, thereby tuning excitability5–7. Cell-type specific expression of such actuators is commonly achieved by combining sophisticated expression systems with specific promoters8, but only few publications report cell compartment-specific expression of optogenetic actuators, including expression in the postsynaptic density9, in dendrites10 and in axon initial segments11,12. While these tools allow manipulation of the local plasma membrane potential, optogenetic tools to control the ion and voltage gradients across intracellular membranes in neurons have not been developed to date. Here we report a strategy to express the light-activated proton pump Archaerhodopsin-3 (Arch3)7,13 from *Halorubrum sodomense* on synaptic vesicles, together with the pH-sensitive GFP variant pHluorin as sensor for vesicular pH14. The fusion protein, named pHoenix, enables controlling and monitoring acidification of synaptic vesicles by yellow and blue light, respectively. We applied pHoenix in order to manipulate the neurotransmitter content of synaptic vesicles and to investigate the interplay of vesicle content and exocytosis. First, we found that additional optogenetic acidification slightly increases EPSC amplitudes, as well as quantal size. Second, we assessed whether insufficient filling of glutamatergic vesicles affects release probability. After pharmacological depletion of the synaptic vesicle content, we subsequently employed pHoenix for optically controlled re-acidification and restoration of transmitter uptake, and found that insufficiently filled vesicles fuse with a lower probability. Based on the modular design of pHoenix, we also created a variant targeting lysosomes, enabling external control of lysosomal acidification.

Results

Targeting Arch3 onto synaptic vesicles

In order to functionally express a light-activated proton pump in the synaptic vesicle membrane, we incorporated Arch3 between helix three and four of the vesicular protein synaptophysin, together with the fluorescent proteins mKate2 on the cytosolic and pHluorin on the luminal side to indicate protein expression and localization as well as luminal acidification. As the C-terminus of Arch3 is located on the cytosolic side13, while the fourth synaptophysin helix originates in the vesicle lumen, we added the transmembrane helix of the rat gastric H^+/K^+ ATPase beta-subunit (βHK) to maintain the transmembrane topology15 (Fig. 1a, Supplementary Fig. 1a,b).

We expressed the resulting fusion protein, pHoenix, in mouse hippocampal neurons using lentivirus. After two weeks in culture, pHoenix was enriched at presynaptic terminals and

colocalized with the vesicular glutamate transporter 1 (VGLUT1), which was not the case for untargeted Arch3-eGFP (Fig. 1b). During whole-cell patch clamp recordings, 1 s light pulses evoked 250 times smaller somatic outward currents in pHoenix-expressing neurons compared to neurons expressing Arch3-eGFP (Fig. 1c), indicating that pHoenix is mostly retained intracellularly. Indeed, optical quantification of surface-resident pHluorin molecules (Supplementary Fig. 1c,d) revealed that only 15% of the pHoenix proteins reside in the plasma membrane (Fig. 1d), similarly to synaptophysin-pHluorin (sypHy), a well-established indicator of vesicular pH and synaptic transmission14. Furthermore, bursts of 60 action potentials (APs) at 20 Hz triggered an increase of pHluorin fluorescence due to exocytosis of synaptic vesicles in pHoenix-expressing neurons (Fig. 1e), demonstrating proper integration of the construct into synaptic vesicles. Notably, expression of pHoenix did not interfere with basic neuronal release parameters (Supplementary Fig. 2).

Light-driven acidification of synaptic vesicles by pHoenix

V-ATPases acidify newly formed synaptic vesicles after their endocytosis from the presynaptic plasma membrane, providing the proton-motive force that drives the neurotransmitter uptake by specialized antiporters such as the vesicular glutamate transporters VGLUT1–316. In order test whether pHoenix can functionally substitute for the activity of the endogenous proton pumps, we blocked vesicular acidification and transmitter uptake by incubating cultured hippocampal neurons grown on microislands with the V-ATPase inhibitor bafilomycin A1 (Baf). We then monitored pHluorin signals in glutamatergic neurons to follow vesicle acidification and, in parallel, recorded excitatory postsynaptic currents (EPSCs), which indicated the level of vesicular transmitter filling. Preincubation with 1 μM Baf for 2–5 h depleted the proton gradient over vesicular membranes and resulted in strong pHluorin fluorescence at synaptic terminals (Fig. 2a), with no or very small EPSCs evoked by APs (Fig. 2b). pHoenix activation with 580 nm light for 2 minutes resulted in a biphasic fluorescence decrease, with an immediate drop to 70% within the first 5 s, reflecting fast vesicle acidification, followed by a slower decay to 60% (Fig. 2a,c). Simultaneously recorded EPSCs recovered with a time constant $\tau = 58$ s (Fig. 2b,c). Control experiments in neurons expressing sypHy showed that bleaching of pHluorin-molecules could not account for the rapid decrease of fluorescence (Supplementary Fig. 3). Thus, pHoenix activity is sufficient to rapidly acidify synaptic vesicles, allowing the control of vesicular transmitter uptake with light.

We further tested the applicability of pHoenix in organotypic brain slices. Adeno-associated virus encoding pHoenix was injected into area CA3 after three to five days *in vitro* (Supplementary Fig. 4a). At >14 days post-infection, we incubated slices with 1 μM Baf overnight, which caused strong pHluorin signals (Supplementary Fig. 4b), and effectively abolished EPSCs. pHoenix activation for 2 min recovered synaptic transmission at associational-commissural fiber synapses (Supplementary Fig. 4c,d), illustrating that the use of pHoenix can also be extended to brain slice preparations and possibly *in vivo* applications.

Refilling of synaptic vesicles by pHoenix should create a finite pool of vesicles that could be subsequently depleted by AP-triggered exocytosis. Indeed, following 2 min of illumination

and pHoenix-mediated recovery of transmission, repetitive stimulation with trains of APs (600 APs over 300 s), but not sparse stimulation (30 APs in 300 s), rapidly reduced EPSC amplitudes in autaptic cultures of glutamatergic neurons (Supplementary Fig. 5). Accordingly, pHluorin signals strongly increased under the train stimulation due to exhaustive exocytosis and failure of re-acidification. A second illumination period caused re-quenching of pHluorin signals, while synaptic transmission recovered, illustrating that optogenetic vesicle acidification and transmitter uptake is fully reversible by AP-driven exocytosis.

The observed rescue of transmission in Baf-treated neurons was pHoenix-specific: While light-induced EPSC recovery in pHoenix-expressing cells yielded EPSCs of 3.1 ± 0.6 nA, illumination failed to rescue EPSCs in control cells expressing Arch3-eGFP (Supplementary Fig. 6a). Rescued EPSCs of Baf-treated neurons reached amplitudes comparable to those of EPSCs of untreated cells from the same culture (Supplementary Fig. 6b). Importantly, the frequency and amplitude of spontaneous miniature EPSCs (mEPSCs), which reflect the stochastic fusion of single vesicles, did not differ between the two groups (Supplementary Fig. 6c). Thus, the light-driven pHoenix activity can achieve vesicular transmitter filling comparable to endogenous V-ATPases.

Superfilling of synaptic vesicles by pHoenix activity

EPSCs of untreated neurons expressing pHoenix slightly increased during illumination (Supplementary Fig. 6b). We characterized this effect in detail by comparing pHoenix-expressing neurons with control neurons (uninfected or sypHy-infected). Activation of pHoenix increased EPSC amplitudes by 13 ± 2%, an effect not seen in controls (Fig. 3a). We directly assessed the release probability in these cells by using a 40 ms paired pulse stimulation paradigm, where a low ratio of the second to first EPSC amplitude indicates a high release probability17. The light-induced change in the paired-pulse ratio (PPR) was not significantly different between the two groups (Fig. 3b), thus the increase of EPSC amplitudes was probably not due to a higher release probability. Likewise, illumination did not have a differential effect on the mEPSC frequency (Fig. 3c). However, illumination caused a significant increase of mEPSCs amplitudes by 11 ± 2% (Fig. 3d) in pHoenix-expressing cells. Our experiments suggest that light-activated proton pumping by pHoenix provides an additional driving force for vesicular transmitter accumulation, reflected by larger postsynaptic responses (Fig. 3e), but the relatively small effect on both EPSC and mEPSC amplitudes implies that vesicles are nearly filled to maximal storage capacity under physiological conditions.

Partially filled vesicles have a lower release probability

Reliable synaptic transmission requires exocytosis of synaptic vesicles loaded with sufficient levels of neurotransmitter molecules. However, whether incomplete vesicular filling affects vesicle release probability is still under debate. In fact, some experimental findings showed that the vesicular fill state influences vesicle release probability18,19, while others demonstrated equally efficient release of empty vesicles20,21. The ability to control transmitter uptake into vesicles by light-driven proton pumping allowed us to directly assess the relation of vesicular transmitter content and vesicular release probability. We

investigated transmitter release of autaptic neurons that still exhibited small, residual EPSCs after >2 h incubation in Baf and compared it to the restored release after pHoenix activation (Fig. 4a). pHoenix-driven transmitter uptake increased mEPSC amplitudes by 70%, while mEPSC frequency increased more than tenfold (Fig. 4b). The small initial mEPSC amplitudes imply that residual EPSCs rely on vesicles only partially filled with glutamate. Notably, the PPR decreased by 40% during the pHoenix-mediated EPSC recovery (Fig. 4c), indicating that vesicular release probability increases with vesicular filling. The incrementing release of glutamate could lead to a progressive desensitization of postsynaptic AMPA receptors, which might contribute to changes in the PPR22. However, in the presence of cyclothiazide, an antagonist of AMPA receptor desensitization, we observed a comparable decrease in PPR (Supplementary Fig. 7), ruling out that in our experimental conditions the increased vesicular content enhances receptor desensitization.

The high PPR of residual EPSCs might result from the release of a pool of "release-reluctant" vesicles that were not discharged during the incubation with Baf because of their intrinsically low release probability. As pHoenix activity promotes gradual filling of synaptic vesicles, we were able to titrate the vesicular glutamate content more accurately using a two-step recovery protocol: In cells devoid of transmission after Baf treatment, we applied a 30 s non-saturating light pulse that caused only partial recovery of the evoked response, followed by a dark phase of 60 s and a second saturating light pulse for 90 s (Fig. 5a). This protocol allowed us to compare an intermediate fill state with reduced postsynaptic responses to the condition with full vesicles after final EPSC recovery. In the intermediate fill state, EPSCs remained stable, at 37% of the final amplitude, while pHluorin signals increased slightly due to AP-triggered exocytosis (Supplementary Fig. 8). This illustrates that VGLUTs require constant proton pumping for transmitter uptake. Using two independent approaches we verified that the non-saturating light pulse created partially filled vesicles: First, analysis of spontaneous release revealed that mEPSC amplitudes were 25% smaller and occurred at a 42% lower frequency compared to the full recovery state (Fig. 5b). Second, we tested the effectiveness of the low-affinity, competitive AMPAR antagonist γ-D-glutamylglycine (γ-DGG) on attenuating EPSCs, which has been established as an indicator for the amount of vesicular glutamate released by exocytosis23: A strong reduction of EPSCs by γ-DGG reflects a low vesicular glutamate content, while the γ-DGG effect decreases with increasing amounts of glutamate released. We found that after the non-saturating light interval, γ-DGG decreased EPSCs to 31%, while EPSCs were reduced to only 40% after the second, saturating light interval (Fig. 5c). Both observations support the idea that the reduced postsynaptic responses in the intermediate recovery are based on a partial vesicular fill state. How does partial transmitter filling affect the release probability? Paired-pulse measurements showed a 10% higher PPR in the intermediate recovery state compared to the full state (Fig. 5d), indicating a lower release probability of partially filled vesicles. We also assessed the readily releasable pool (RRP) of synaptic vesicles by brief applications of hypertonic sucrose solutions during the intermediate and the final recovery state (Fig. 5e,f), which allowed us to directly calculate the vesicular release probability (P_{vr})24. During the intermediate recovery state the RRP was 60% smaller compared to the final recovery state (Fig. 5g,i). The P_{vr} of partially filled vesicles was 14% lower compared to vesicles after

complete filling (Fig. 5h,i), and the vesicular fill state correlated with the pool size and P_{vr} (Fig. 5j). Thus, insufficient vesicular filling reduces the vesicular release probability.

Light-driven acidification of lysosomes

The modular pHoenix design provides a blueprint for specific intracellular trafficking of both Arch3 and fluorescent indicators. Consequently, we modified pHoenix to target lysosomes by insertion of the pHluorin-Arch3-mKate-βHK construct between helix 1 and 2 of the tetraspanin CD63, a lysosomal marker protein25 (Fig. 6a). The resulting "lyso-pHoenix" showed strong co-labeling with the lysosome-associated membrane protein 2 (LAMP2), but not with markers for the Golgi apparatus, endoplasmic reticulum, endosome, or mitochondria, demonstrating specific expression on lysosomal membranes (Fig. 6c, Supplementary Fig. 9). In Baf-treated HEK 293 cells, activation of lyso-pHoenix by 580 nm light caused a rapid decrease of pHluorin signals, indicating a drop in pH, which was not seen in control cells expressing CD63-pHluorin. Remarkably, lysosomal acidification required constant proton pumping, as pHluorin signals quickly recovered after termination of lyso-pHoenix activation, suggesting a strong proton leak in lysosomes (Fig. 6d).

Discussion

Light-driven proton pumps are powerful tools for silencing neuronal activity, as they hyperpolarize the plasma membrane by exporting protons from the cytosol to the extracellular side of the membrane26. Interestingly, only few studies have exploited their potential to alter the pH of intracellular organelles. In yeast, the light-driven proton pump bacteriorhodopsin from *Halobacterium salinarium* has been successfully targeted to the inner mitochondrial membrane27. In cell-free assays, bacteriorhodopsin from *Halobacterium halobium* has been employed to acidify proteoliposomes in order to study the proton-dependence of VGLUT-driven glutamate uptake28, but similar experiments have not yet been feasible in living neurons. Our new tool, pHoenix, now allows precise temporal control of the acidification process of synaptic vesicles, and will enable studies on synaptic vesicle biogenesis and neurotransmitter uptake in living neurons.

Two parameters affect the vesicular transmitter filling: the proton gradient and the number and activity of vesicular transmitter transporters. Experimentally, the vesicular transmitter content can be manipulated in two ways – either by altering the number of active vesicular transmitter transporters19,29–31, or by alteration of the proton electrochemical gradient20,21. To our knowledge, pHoenix is the first tool enabling acute increase of the vesicular proton-gradient. In cells with intact V-ATPase function, additional optogenetic acidification increased both EPSC and mEPSC amplitudes by more than 10%. The ability of pHoenix to increase the vesicular glutamate filling beyond the filling capacity provided by V-ATPases demonstrates that Arch3 generates a proton motive force that exceeds the driving force provided by endogenous V-ATPases, indicating that the proton transport properties of V-ATPases limit the amount of glutamate uptake. The EPSC and mEPSC amplitude increase by pHoenix activation in untreated neurons also implies that activation of surface resident pHoenix does not cause significant synaptic cleft acidification, which would impair synaptic

transmission by inhibiting presynaptic calcium influx through voltage gated calcium channels32.

In Baf-treated neurons, refilling of vesicles by interval illumination revealed that glutamate uptake requires constant proton pumping (Supplementary Fig. 8). While pH remained low, glutamate uptake stopped immediately after light off and cessation of pHoenix activity. This is strong evidence for the notion that membrane voltage and not the pH gradient is the driving-force for VGLUT-mediated transmitter uptake2. The absence of proton leakage and stable synaptic transmission during low-frequency stimulation indicates that both low luminal pH and transmitter content of glutamatergic synaptic vesicles are preserved even in the absence of V-ATPase function, arguing against a steady-state model of transmitter uptake and leak in synaptic vesicles33. This is not the case for lysosomes, where the pH increased again within seconds after terminating the lyso-pHoenix-mediated acidification, demonstrating constant lysosomal proton leakage.

Our experiments further revealed that partially filled neurotransmitter vesicles can be released, proving that exocytosis is not guarded by a rigid fill-state control mechanism. However, incompletely filled vesicles do have a lower release probability. The underlying mechanism for this observation is not clear, but it seems likely that proton pumping and transmitter accumulation increase intravesicular osmolarity, which leads to a higher vesicle membrane tension and increases fusion probability with the plasma membrane. Electron microscopy studies revealed that synaptic vesicles of VGLUT1 deficient neurons were deformed in contrast to vesicles from wildtype neurons, suggesting that failure of transmitter uptake (but not failure of acidification) renders them more labile19,34. Moreover, filled vesicles were found to exhibit a larger diameter than empty vesicles35,36. Interestingly, the PPR changed faster than EPSCs increased, both at high (Fig. 4) and low illumination intensity (Supplementary Fig. 7), indicating that the threshold for a high P_{vr} defined by intravesicular osmolarity and membrane tension is reached before the maximal vesicular transmitter storage capacity. In line with this, we observed no further increase of the release probability when we used pHoenix in untreated cells to further increase vesicular filling (Fig. 3). The preferential release of completely filled vesicles could be of relevance for synaptic information processing: During sustained neuronal firing and high turnover of vesicles, this mechanism might assure efficient postsynaptic receptor activation and reliable synaptic transmission.

As pHoenix can functionally replace V-ATPases, it can be applied to rescue the cellular degeneration observed in V-ATPase KO models in yeast37, Drosophila38, and mice39. Recent studies suggested that V-ATPases have acidification-independent functions as vesicular pH-sensors40, interaction partners of SNARE proteins41, and may participate directly in synaptic vesicle fusion42. In combination with pump activity-deficient V-ATPase mutants43, pHoenix will facilitate structure–function analyses of V-ATPases and help to elucidate their non-canonical roles.

Optogenetic organelle acidification allows to investigate quantitative aspects of proton-dependent transport and to study the properties of organelles as a function of their intraluminal pH. To further pursue this goal we aimed to develop a variant with opposing

function to pHoenix by replacing Arch3 by a channelrhodopsin with high proton conductance in order to deplete proton gradients using light. Unfortunately, all tested channelrhodopsin-derived pHoenix variants were ineffective (data not shown), probably because the multimerization properties of channelrhodopsins and microbial pumps differ[44–46]. In line with this, a pHoenix-based actuator that allows manipulation of circuit activity will require further developments of the construct.

Whereas the transfer of the pHoenix concept to other microbial-type rhodopsins has proven unsuccessful to date, we were able to target a pHoenix variant to a different subcellular compartment by replacing the synaptophysin parts in pHoenix with the lysosomal CD63 protein. The resulting lyso-pHoenix can be applied to specifically investigate the pH-dependency of the catabolic processes confined to lysosomes, e.g. the acid-dependent activity of lysosomal proteases[47]. Notably, alterations in organelle pH-homeostasis due to defects in proton translocation or counterion conductances are associated with many different pathophysiological conditions[48], ranging from cancer[49] to neurodegeneration[50]. The here presented pHoenix-constructs may provide a new approach for directly assessing the role of acidification in these disorders.

Online Methods

Cloning strategy and virus production

To generate the pHoenix construct, we inserted Archaerhodopsin-3 (Arch3) from *Halorubrum sodomense* into the synaptophysin molecule. Since it has been reported that a sypHy version lacking the fourth transmembrane domain and thus the C-terminus of synaptophysin was incorrectly targeted in neurons[51], we maintained the N- and C-terminus of synaptophysin as trafficking signals. First, we inserted a single transmembrane domain of the rat gastric H^+/K^+ ATPase beta-subunit[52], which had previously been successfully used for tandem optogenetic constructs[15], into the rat synaptophysin-pHluorin 2x (sypHy2) construct[53] using Age I sites, thereby replacing the second superecliptic pHluorin molecule. Next, we amplified Arch3 cDNA (from Addgene clone 22222) by PCR. The fragment was inserted C-terminal to the super-ecliptic pHluorin using BamHI and SplI sites. Finally, the red fluorescent marker mKate2[54] was inserted at the cytosolic C-terminus of Arch3 via SplI and HindIII.

CD63 cDNA was generated by TA cloning from mouse whole brain mRNA and transferred into a mammalian expression vector with CMV promoter. As the large second luminal loop contains three potential N-linked glycosylation motives[25], we introduced AfeI and SacI restriction sites into the first luminal loop as insertion site for the optogenetic cassette encoding pHluorin, Arch3, mKate2 and the rat gastric H^+/K^+ ATPase beta-subunit. In order to create CD63-pHluorin, the CD63-pHoenix construct was AgeI-digested, thereby removing Arch3, mKate2 and the H^+/K^+ ATPase beta-subunit, and religated. All constructs were verified by sequencing. Plasmids encoding pHoenix (Genbank accession number KT880224), lyso-pHoenix (Genbank accession number KT880225) and lyso-pHluorin (Genbank accession number KT880226) can be obtained via Addgene.

Viral particles were provided by the Viral Core Facility (VCF) of the Charité Berlin. Lentivirus was produced according to published protocols55, with minor modifications: The coding sequences of pHoenix, sypHy (Addgene clone 24478) or Arch3-EGFP were transferred into a modified FUGW lentiviral expression vector55 with the neuron-specific human synapsin promoter. 20 Mg of the expression vector were cotransfected into HEK 293T cells with 5 Mg each of the helper plasmids pCMVdR8.9 and pVSV.G using X-tremeGENE 9 DNA transfection reagent (Roche). Lentiviral particles were harvested from cultures maintained in Neurobasal-A supplemented with 2% B27 and 0.2% penicillin/ streptomycin (all cell culture media from Invitrogen) at 32 °C and 5% CO_2 for 72 h. Supernatants were filtered and subsequently 20x concentrated using Amicon Ultra-15 centrifugal 10 kDa filter units. Aliquots of the lentivirus were shock-frozen and stored at –80 °C. Adeno-associated virus (AAV) serotype 9 was produced in HEK293 cells transfected with polyethylenimine (PEI) and the following plasmids: pAD deltaF6, pAAV2/9 (both from Penn Vector Core, University of Pennsylvania) and an AAV expression vector encoding pHoenix under the human synapsin promoter. After 48 h, cells were resuspended, collected by centrifugation and lysed in 50 mM Tris-Cl, 150 mM NaCl. Viral particles were purified using an iodixanol gradient purification process according to published protocols56 and stored at 4 °C.

Cell culture

Animals were handled in accordance with the regulations of local authorities and the animal welfare committee of the Charité – Universitätsmedizin Berlin, Germany.

Autaptic cultures of primary hippocampal neurons: Low-density cultures of hippocampal neurons on glia cell microislands57 were prepared from newborn C57/BL6-N mice of either sex as previously described58. Briefly, astrocytes were prepared from cortices and expanded in T75 bottles in Dulbecco's Modified Eagle Medium (DMEM) supplemented with 10% fetal calf serum and 0.2% penicillin/streptomycin (Invitrogen). To obtain microisland cultures, coverslips were coated with a thin film of agarose. After drying the agarose, a pattern of 300 μm diameter spots of growth permissive substrate consisting of 0.7 mg ml^{-1} collagen and 0.1 mg ml^{-1} poly-D-lysine was applied using a custom-made stamp. After 14 days in vitro (DIV) astrocytes were seeded onto the glass coverslips at a density of 5000 cm^{-2}, and were allowed to proliferate in DMEM medium for one more week to form microislands. Medium was changed to Neurobasal-A supplemented with 2% B27 and 0.2% penicillin/ streptomycin 24 h before hippocampal neurons prepared from P0 mice were added at a density of 300 cm^{-2}. Neurons were infected with lentiviral particles at DIV 1–2.

Cultures of HEK 293 and HeLa cells: Cell lines were maintained in DMEM supplemented with 10% fetal calf serum and 0.2% penicillin/streptomycin. For live-cell imaging and immunocytochemistry experiments, cells were seeded at low density onto coverslips coated with 0.7 mg ml^{-1} collagen and 0.1 mg ml^{-1} poly-D-lysine, transfected after 24 h using X-tremeGENE 9 DNA transfection reagent according to the manufacturer's instructions, and were used 24–48 h post transfection.

Hippocampal organotypic slice cultures: Wistar rat hippocampi were dissected from pups of either sex (postnatal day 5–8) in a sucrose-based solution and horizontal slices were cut

using a vibratome (Leica VT1200S). Slices were washed with sterile solution and plated on membrane inserts (0.4 μm Millicell, Millipore). Culture medium contained 50% Basal Medium Eagles (BME), 25% Hank's balanced salt solution (HBSS), 25% heat-inactivated horse serum, 1 mM Glutamax I supplement (all from GIBCO), and 6.5 g/L D-glucose. Antibiotics were added 24 h after the preparation (penicillin/streptomycin). The medium was changed three times a week, no antimycotics were used. At DIV 3–5 slices were transduced under sterile conditions with an AAV encoding pHoenix using a micromanipulator. The tip of a baked pipette was filled with the AAV-containing solution and lowered into stratum pyramidale of area CA3 so that the virus could diffuse into the slice.

Electrophysiology

Experiments on autaptic neurons were performed at room temperature on an Olympus IX51 inverted microscope equipped with a Multiclamp 700B amplifier under control of a Digidata 1440 AD board and pClamp10 software (Molecular Devices). External solutions were applied using a custom-built rapid perfusion system58, while the bath level was controlled by an MPCU bath handler (Lorenz Messgerätebau, Katlenburg-Lindau, Germany). Whole-cell recordings were performed between DIV14 and 21. Cells were voltage clamped at –70 mV, with 70% compensation of series resistance and capacitance. Recordings were discarded when the series resistance exceeded 15 MOhm. To evoke EPSCs in autaptic neurons, unclamped action potentials were triggered by a 1-ms depolarization step to 0 mV. Spontaneous mEPSCs were analyzed from the same recordings in intervals starting 2 s after the action potential. Intracellular solution contained (in mM): 135 potassium gluconate, 17.8 Hepes, 1 EGTA, 4.6 $MgCl_2$, 4 Na_2ATP, 12 creatine phosphate and 50 U/ml creatine phosphokinase, pH adjusted to 7.3 with KOH, 300 mOsm. Cells were continuously superfused with HEPES-buffered solution (in mM): 140 NaCl, 2.4 KCl, 10 HEPES, 10 glucose, 2 $CaCl_2$, and 4 $MgCl_2$, pH adjusted to 7.3 with NaOH, 300 mOsm. The readily releasable pool was determined as the charge transient of the postsynaptic current evoked by a 5-s application of 500 mM sucrose dissolved in extracellular solution, and the P_{vr} was calculated as the ratio of the EPSC charge and the sucrose-evoked charge24. The antagonist for AMPAR-desensitization cyclothiazide (Tocris) was used at 100 μM, and the low affinity AMPAR antagonist γ-D-glutamylglycine (γ-DGG) at 500 μM. Data were sampled at 10 kHz and filtered at 3 kHz. Cultures were treated for 2–5 h with 1 μM bafilomycin A1 (Tocris, Bristol, UK; or Enzo Life Sciences, Farmingdale, NY, USA) before the recordings.

Hippocampal organotypic slice cultures were transferred to a submerged recording chamber on an upright Olympus BX51 microscope and continuously perfused with ACSF (in mM): 125 NaCl, 25 $NaHCO_3$, 3 KCl, 1.25 NaH_2PO_4, 2 $CaCl_2$, 1 $MgCl_2$, and 10 glucose, oxygenated at 95% O_2 and 5% CO_2. Whole-cell recordings from CA3 neurons were performed at room temperature with an Axon Multiclamp 700B amplifier. Intracellular solution contained (in mM): 135 potassium gluconate, 7 NaCl, 10 HEPES, 2 Na_2ATP, 0.3 Na-GTP and 2 $MgCl_2$, pH adjusted to 7.2–7.3 with KOH. The stimulation electrode was placed in stratum radiatum and APs were triggered at 0.1 Hz. Stimulus intensities were adjusted to values similar to those used in control slices without treatment of Baf.

Light delivery and live-cell imaging

In electrophysiological experiments on autaptic neurons without imaging, we activated pHoenix using a mercury lamp for illumination controlled by a TTL-controlled mechanical shutter (Uniblitz, Vincent Associates, NY, USA). Excitation light was passed through a 25% neutral density filter (Olympus) and a 546/10 nm excitation filter (11002v2-Green, Chroma Technology, Bellows Falls, VT, USA). The light intensity above the objective (Olympus UPLSAPO 20X, 0.75 NA) was 265 mW cm^{-2} at 546 nm. Similarly, organotypic hippocampal slices were illuminated through the objective (Olympus LumPlan FI 60X, 0.9 NA water immersion) with a mercury lamp controlled by a TTL-driven mechanical shutter, using a 587/25 nm excitation filter (F20-451, AHF Analysentechnik, Tübingen, Germany).

For electrophysiology experiments and parallel imaging of pHluorin signals in autaptic neurons we used an Olympus UPLSAPO 60X, 1.2 NA water immersion objective. A TTL-controlled LED system (pE2, CoolLED, Andover, UK) equipped with a 490-nm LED and a broadband "GYR" LED was coupled into the backport of the microscope. Excitation and emission light was separated by a multiband dichroic mirror (F72-628, AHF Analysentechnik, Tübingen, Germany). We found that band-pass filters (blue LED: excitation filter of the AHF Tripleband Filterset F69-402 with 495/10; GYR-LED: AHF F47-605 with 605/70) prevented unintended Arch3 activation by the blue LED, and allowed optimal Arch3-activation and minimized bleaching of pHluorin molecules by the yellow LED. Fluorescence signals of pHluorin molecules were bandpass filtered (AHF F73-402) and imaged with an EMCCD camera (iXon 897, Andor, Belfast, UK) using the Micromanager software59. During reacidification experiments, pHluorin signals were captured at 0.2 Hz, except for experiments in Supplementary Fig. 4 (0.05 Hz). After acquisition of baseline pHluorin signals, pHoenix was activated by a near-continuous illumination with the GYR-LED, which was briefly interrupted at 0.2 or 0.05 Hz by 100 ms flashes of the 490 nm LED. The following LED settings were applied for these imaging experiments: 490 nm LED set to 10–20% (50–100 mW cm^{-2}); GYR-LED set to 100% (1100 mW cm^{-2} at 580 nm), 4.8 or 19.8 s exposure at 0.2 or 0.05 Hz respectively. GYR-LED was set to 10% for low light intensity experiments presented in Supplementary Fig. 7. Intensities were measured above the objective. For the EMCCD we used the following settings: 100 ms exposure synchronized with the 490 nm LED, 2x2 bin, –80 °C, 4.7x pregain; EMgain 300 for pHoenix imaging, 100 for sypHy imaging. The same imaging setup was used for experiments on HEK 293 cells expressing lyso-pHoenix.

We determined the fraction of surface-resident pHoenix or sypHy molecules by applying an extracellular solution buffered with 10 mM MES instead of HEPES at pH 5.5, followed by the application of 50 mM NH_4Cl containing extracellular solution with NaCl reduced to 90 mM to maintain the osmolarity60. Images were acquired at 2 Hz during the pH 5.5 – NH_4 protocol.

Immunocytochemistry

High-density cultures of pHoenix and Arch3 expressing hippocampal neurons were fixed at DIV 14 with 3% (w/v) paraformaldehyde for 10–15 minutes at room temperature. Fixed samples were stained with primary antibodies against VGLUT1 (#135 302, Synaptic

Europe PMC Funders Author Manuscripts

Systems, Göttingen, Germany) and MAP2 (AB5543, Chemicon by Merck Millipore, Darmstadt, Germany) and secondary antibodies coupled to Alexa Fluor 647 or Dylight-405 (#711-605-152 and #711-475-152, respectively, Jackson ImmunoResearch, West Grove, PA, USA). Stained samples were mounted in Mowiol. Fluorescent specimens were examined under a confocal laser-scanning microscope (TCS SP5, Leica, Wetzlar, Germany). 1024 x 1024 pixel images were acquired using a 63X, 1.4 NA oil immersion objective and a 2–4x zoom.

Lyso-pHoenix transfected HeLa cells were fixed 24 h after transfection with 4% (w/v) paraformaldehyde for 12 minutes at room temperature or with methanol for 15 minutes at –20 °C. The following primary antibodies were used: Primary antibodies against GFP (#A-11122, Life Technologies), human CD107b (lysosome-associated membrane protein-2, LAMP-2; #10-672-C100, HISS Diagnostics), human Rab-5 (#108011, Synaptic Systems), human PDI (#MA 3-019, Affinity BioReagents), human GM-130 (#610823, BD Biosciences) and human Hsp-60 (#611563, BD Biosiences). Secondary antibodies were coupled to Alexa 488 (#A11034) and Alexa 633 (#A21052, both Life Technologies, Molecular Probes, Carlsbad, CA, USA) respectively. For imaging, the cells were mounted with Aqua Poly Mount (#633736, Polysciences, Warrington, PA, USA). Images were acquired with a laser-scanning confocal microscope (LSM510, Carl Zeiss, Jena, Germany) equipped with a 63X, 1.4 NA oil immersion objective. The image size was set to 1024 x 1024 pixels. Images for figures were processed with ImageJ software (ImageJ 1.47t; NIH, USA) to enhance brightness using the brightness/contrast function. Immunocytochemistry experiments were repeated two to three times.

Data collection and analysis

Viral particles encoding controls and pHoenix constructs were randomly applied on different wells of the same 6- or 12 well plates from the same culture. From each culture, wells were randomly subjected to treatment or control conditions, and recordings from multiple groups were performed on the same day, in a randomized order. Data collection and analysis were not performed blind to the conditions of the experiments.

Electrophysiological recordings were analyzed using the AxographX software. For mEPSC analysis, we used the implemented scaled template detection algorithm for recordings that had been filtered once post-hoc with a 1 kHz low-pass filter. False-positive events were estimated by running the spontaneous event detection with an inverted template61. Frequency and amplitude of mEPSCs were corrected for false-positives, and recordings with false-positive events of > 2 Hz were excluded.

Images of pHluorin signals were analyzed using ImageJ and the Time Series Analyzer V2.0 plug-in. Fluorescence intensities were calculated from 2x2 pixel regions of interest (ROI) drawn on synaptic contacts, which were identified as small structures with a dynamic increase of fluorescence evoked by NH_4 application. Background fluorescence from a region with no neuronal structures was subtracted for each frame.

Colocalization of lyso-pHoenix and organelle markers was analyzed using the CellProfiler 2.1.1 program (Broad Institute of MIT and Harvard)62. In a pixel-based approach the

colocalization of two channels was calculated after the images were aligned. For every co-staining ten cells were analyzed and the Pearson's correlation coefficient was determined.

Data are presented as mean ± SEM and were tested for normality using the D'Agostino and Pearson omnibus normality test. Sample sizes were not predetermined by statistical methods, but are similar to those reported in comparable previous publications15. Time constants were calculated from fitting the data as monoexponential decay or association using GraphPad Prism 5. Differences between two groups were tested for significance by unpaired or paired two-way Student's *t*-tests. If data did not pass the normality test we applied a Mann-Whitney *U* test for unpaired and a Wilcoxon signed-rank test for paired data. For multiple comparisons of EPSC amplitudes and mEPSC frequencies in Supplementary Fig. 5, we used repeated measures two-way ANOVA with Sidak's multiple comparisons post-test, and a regular two-way ANOVA with Sidak's multiple comparisons post-test for comparisons of mEPSC amplitudes (due to three Baf-treated cells without detectable mEPSCs in the pre-light condition, repeated measures two-way ANOVA could not be performed for mEPSC amplitudes). Number of cells (*n*) and number of cultures (*N*) are reported in the figure legends. Statistics were calculated using GraphPad Prism 5 and 6.

Supplementary Material

Refer to Web version on PubMed Central for supplementary material.

Acknowledgments

We thank Katja Rösler, Bettina Brokowski, Annegret Felies, Berit Söhl-Kielczynski, Carola Schweynoch, Jelena Pustogowa and Anke Schönherr for excellent technical support, the viral core facility of the Charité for virus production, and Marcial Camacho-Perez, Shigeki Watanabe and Ari Liebkowsky for critical comments on the manuscript. The work was supported by the German Research Council grants Cluster of Excellence Neurocure (EXC 257), Collaborative Research Center SFB958 (D.S.; C.R.), Collaborative Research Center SFB1078 (F.S.; P.H.), and the Integrative Research Institute (IRI) for the Life Sciences (D.S.; P.H.; C.R.), a European Research Council grant (249939 SYNVGLUT; C.R.), a Grass Foundation Fellowship (B.R.R.), and the Louis-Jeantet Foundation (F.S.; P.H.).

References

1. Blakely RD, Edwards RH. Vesicular and plasma membrane transporters for neurotransmitters. Cold Spring Harb Perspect Biol. 2012; 4
2. Omote H, Miyaji T, Juge N, Moriyama Y. Vesicular neurotransmitter transporter: bioenergetics and regulation of glutamate transport. Biochemistry. 2011; 50:5558–5565. [PubMed: 21612282]
3. Mindell JA. Lysosomal acidification mechanisms. Annu Rev Physiol. 2012; 74:69–86. [PubMed: 22335796]
4. Forgac M. Vacuolar ATPases: rotary proton pumps in physiology and pathophysiology. Nat Rev Mol Cell Biol. 2007; 8:917–929. [PubMed: 17912264]
5. Boyden ES, Zhang F, Bamberg E, Nagel G, Deisseroth K. Millisecond-timescale, genetically targeted optical control of neural activity. Nat Neurosci. 2005; 8:1263–1268. [PubMed: 16116447]
6. Han X, Boyden ES. Multiple-color optical activation, silencing, and desynchronization of neural activity, with single-spike temporal resolution. PLoS One. 2007; 2:e299. [PubMed: 17375185]
7. Chow BY, et al. High-performance genetically targetable optical neural silencing by light-driven proton pumps. Nature. 2010; 463:98–102. [PubMed: 20054397]
8. Yizhar O, Fenno LE, Davidson TJ, Mogri M, Deisseroth K. Optogenetics in neural systems. Neuron. 2011; 71:9–34. [PubMed: 21745635]

Europe PMC Funders Author Manuscripts

9. Gradinaru V, et al. Targeting and readout strategies for fast optical neural control in vitro and in vivo. J Neurosci. 2007; 27:14231–14238. [PubMed: 18160630]
10. Greenberg KP, Pham A, Werblin FS. Differential targeting of optical neuromodulators to ganglion cell soma and dendrites allows dynamic control of center-surround antagonism. Neuron. 2011; 69:713–720. [PubMed: 21338881]
11. Grubb MS, Burrone J. Channelrhodopsin-2 localised to the axon initial segment. PLoS One. 2010; 5:e13761. [PubMed: 21048938]
12. Wu C, Ivanova E, Cui J, Lu Q, Pan ZH. Action potential generation at an axon initial segment-like process in the axonless retinal AII amacrine cell. J Neurosci. 2011; 31:14654–14659. [PubMed: 21994381]
13. Ihara K, et al. Evolution of the archaeal rhodopsins: evolution rate changes by gene duplication and functional differentiation. J Mol Biol. 1999; 285:163–174. [PubMed: 9878396]
14. Miesenbock G, De Angelis DA, Rothman JE. Visualizing secretion and synaptic transmission with pH-sensitive green fluorescent proteins. Nature. 1998; 394:192–195. [PubMed: 9671304]
15. Kleinlogel S, et al. A gene-fusion strategy for stoichiometric and co-localized expression of light-gated membrane proteins. Nat Methods. 2011; 8:1083–1088. [PubMed: 22056675]
16. Takamori S. VGLUTs: 'exciting' times for glutamatergic research? Neurosci Res. 2006; 55:343–351. [PubMed: 16765470]
17. Regehr WG. Short-term presynaptic plasticity. Cold Spring Harb Perspect Biol. 2012; 4:a005702. [PubMed: 22751149]
18. Wang L, Tu P, Bonet L, Aubrey KR, Supplisson S. Cytosolic transmitter concentration regulates vesicle cycling at hippocampal GABAergic terminals. Neuron. 2013; 80:143–158. [PubMed: 24094108]
19. Herman MA, Ackermann F, Trimbuch T, Rosenmund C. Vesicular Glutamate Transporter Expression Level Affects Synaptic Vesicle Release Probability at Hippocampal Synapses in Culture. The Journal of Neuroscience. 2014; 34:11781–11791. [PubMed: 25164673]
20. Cousin MA, Nicholls DG. Synaptic vesicle recycling in cultured cerebellar granule cells: role of vesicular acidification and refilling. J Neurochem. 1997; 69:1927–1935. [PubMed: 9349537]
21. Zhou Q, Petersen CC, Nicoll RA. Effects of reduced vesicular filling on synaptic transmission in rat hippocampal neurones. J Physiol. 2000; 525(Pt 1):195–206. [PubMed: 10811737]
22. Heine M, et al. Surface mobility of postsynaptic AMPARs tunes synaptic transmission. Science. 2008; 320:201–205. [PubMed: 18403705]
23. Liu G, Choi S, Tsien RW. Variability of neurotransmitter concentration and nonsaturation of postsynaptic AMPA receptors at synapses in hippocampal cultures and slices. Neuron. 1999; 22:395–409. [PubMed: 10069344]
24. Rosenmund C, Stevens CF. Definition of the readily releasable pool of vesicles at hippocampal synapses. Neuron. 1996; 16:1197–1207. [PubMed: 8663996]
25. Metzelaar MJ, et al. CD63 antigen. A novel lysosomal membrane glycoprotein, cloned by a screening procedure for intracellular antigens in eukaryotic cells. J Biol Chem. 1991; 266:3239–3245. [PubMed: 1993697]
26. Mattis J, et al. Principles for applying optogenetic tools derived from direct comparative analysis of microbial opsins. Nat Methods. 2012; 9:159–172. [PubMed: 22179551]
27. Hoffmann A, Hildebrandt V, Heberle J, Buldt G. Photoactive mitochondria: in vivo transfer of a light-driven proton pump into the inner mitochondrial membrane of Schizosaccharomyces pombe. Proc Natl Acad Sci U S A. 1994; 91:9367–9371. [PubMed: 7937771]
28. Maycox PR, Deckwerth T, Jahn R. Bacteriorhodopsin drives the glutamate transporter of synaptic vesicles after co-reconstitution. EMBO J. 1990; 9:1465–1469. [PubMed: 1970294]
29. Moechars D, et al. Vesicular glutamate transporter VGLUT2 expression levels control quantal size and neuropathic pain. J Neurosci. 2006; 26:12055–12066. [PubMed: 17108179]
30. Pothos EN, et al. Synaptic vesicle transporter expression regulates vesicle phenotype and quantal size. J Neurosci. 2000; 20:7297–7306. [PubMed: 11007887]

31. Wojcik SM, et al. An essential role for vesicular glutamate transporter 1 (VGLUT1) in postnatal development and control of quantal size. Proc Natl Acad Sci U S A. 2004; 101:7158–7163. [PubMed: 15103023]
32. Palmer MJ, Hull C, Vigh J, von Gersdorff H. Synaptic cleft acidification and modulation of short-term depression by exocytosed protons in retinal bipolar cells. J Neurosci. 2003; 23:11332–11341. [PubMed: 14672997]
33. Williams J. How does a vesicle know it is full? Neuron. 1997; 18:683–686. [PubMed: 9182793]
34. Siksou L. A role for vesicular glutamate transporter 1 in synaptic vesicle clustering and mobility. Eur J Neurosci. 2013; 37:1631–1642. [PubMed: 23581566]
35. Budzinski KL, et al. Large structural change in isolated synaptic vesicles upon loading with neurotransmitter. Biophys J. 2009; 97:2577–2584. [PubMed: 19883601]
36. Daniels RW, et al. Increased expression of the Drosophila vesicular glutamate transporter leads to excess glutamate release and a compensatory decrease in quantal content. J Neurosci. 2004; 24:10466–10474. [PubMed: 15548661]
37. Nelson H, Nelson N. Disruption of genes encoding subunits of yeast vacuolar H(+)-ATPase causes conditional lethality. Proc Natl Acad Sci U S A. 1990; 87:3503–3507. [PubMed: 2139726]
38. Davies SA, et al. Analysis and inactivation of vha55, the gene encoding the vacuolar ATPase B-subunit in Drosophila melanogaster reveals a larval lethal phenotype. J Biol Chem. 1996; 271:30677–30684. [PubMed: 8940044]
39. Inoue H, Noumi T, Nagata M, Murakami H, Kanazawa H. Targeted disruption of the gene encoding the proteolipid subunit of mouse vacuolar H(+)-ATPase leads to early embryonic lethality. Biochim Biophys Acta. 1999; 1413:130–138. [PubMed: 10556625]
40. Poea-Guyon S, et al. The V-ATPase membrane domain is a sensor of granular pH that controls the exocytotic machinery. J Cell Biol. 2013; 203:283–298. [PubMed: 24165939]
41. Di Giovanni J, et al. V-ATPase membrane sector associates with synaptobrevin to modulate neurotransmitter release. Neuron. 2010; 67:268–279. [PubMed: 20670834]
42. Hiesinger PR, et al. The V-ATPase V0 subunit a1 is required for a late step in synaptic vesicle exocytosis in Drosophila. Cell. 2005; 121:607–620. [PubMed: 15907473]
43. Kawasaki-Nishi S, Nishi T, Forgac M. Arg-735 of the 100-kDa subunit a of the yeast V-ATPase is essential for proton translocation. Proc Natl Acad Sci U S A. 2001; 98:12397–12402. [PubMed: 11592980]
44. Kato HE, et al. Crystal structure of the channelrhodopsin light-gated cation channel. Nature. 2012; 482:369–374. [PubMed: 22266941]
45. Muller M, Bamann C, Bamberg E, Kuhlbrandt W. Projection structure of channelrhodopsin-2 at 6 A resolution by electron crystallography. J Mol Biol. 2011; 414:86–95. [PubMed: 22001017]
46. Yoshimura K, Kouyama T. Structural role of bacterioruberin in the trimeric structure of archaerhodopsin-2. J Mol Biol. 2008; 375:1267–1281. [PubMed: 18082767]
47. Pungercar JR, et al. Autocatalytic processing of procathepsin B is triggered by proenzyme activity. FEBS J. 2009; 276:660–668. [PubMed: 19143833]
48. Weisz OA. Organelle acidification and disease. Traffic. 2003; 4:57–64. [PubMed: 12559032]
49. Jiang LW, Maher VM, McCormick JJ, Schindler M. Alkalinization of the lysosomes is correlated with ras transformation of murine and human fibroblasts. J Biol Chem. 1990; 265:4775–4777. [PubMed: 1690732]
50. Dehay B, et al. Loss of P-type ATPase ATP13A2/PARK9 function induces general lysosomal deficiency and leads to Parkinson disease neurodegeneration. Proc Natl Acad Sci U S A. 2012; 109:9611–9616. [PubMed: 22647602]
51. Royle SJ, Granseth B, Odermatt B, Derevier A, Lagnado L. Imaging phluorin-based probes at hippocampal synapses. Methods Mol Biol. 2008; 457:293–303. [PubMed: 19066036]
52. Shull GE. cDNA cloning of the beta-subunit of the rat gastric H,K-ATPase. J Biol Chem. 1990; 265:12123–12126. [PubMed: 2165052]
53. Zhu Y, Xu J, Heinemann SF. Two pathways of synaptic vesicle retrieval revealed by single-vesicle imaging. Neuron. 2009; 61:397–411. [PubMed: 19217377]

54. Shcherbo D, et al. Far-red fluorescent tags for protein imaging in living tissues. Biochem J. 2009; 418:567–574. [PubMed: 19143658]

55. Lois C, Hong EJ, Pease S, Brown EJ, Baltimore D. Germline transmission and tissue-specific expression of transgenes delivered by lentiviral vectors. Science. 2002; 295:868–872. [PubMed: 11786607]

56. Lock M, et al. Rapid, simple, and versatile manufacturing of recombinant adeno-associated viral vectors at scale. Hum Gene Ther. 2010; 21:1259–1271. [PubMed: 20497038]

57. Bekkers JM, Stevens CF. Excitatory and inhibitory autaptic currents in isolated hippocampal neurons maintained in cell culture. Proc Natl Acad Sci U S A. 1991; 88:7834–7838. [PubMed: 1679238]

58. Rost BR, et al. Autaptic cultures of single hippocampal granule cells of mice and rats. Eur J Neurosci. 2010; 32:939–947. [PubMed: 20726880]

59. Edelstein A, Amodaj N, Hoover K, Vale R, Stuurman N. Computer control of microscopes using microManager. Curr Protoc Mol Biol. 2010 Chapter 14, Unit14 20.

60. Sankaranarayanan S, De Angelis D, Rothman JE, Ryan TA. The use of pHluorins for optical measurements of presynaptic activity. Biophys J. 2000; 79:2199–2208. [PubMed: 11023924]

61. Clements JD, Bekkers JM. Detection of spontaneous synaptic events with an optimally scaled template. Biophys J. 1997; 73:220–229. [PubMed: 9199786]

62. Carpenter AE, et al. CellProfiler: image analysis software for identifying and quantifying cell phenotypes. Genome Biol. 2006; 7:R100. [PubMed: 17076895]

Europe PMC Funders Author Manuscripts

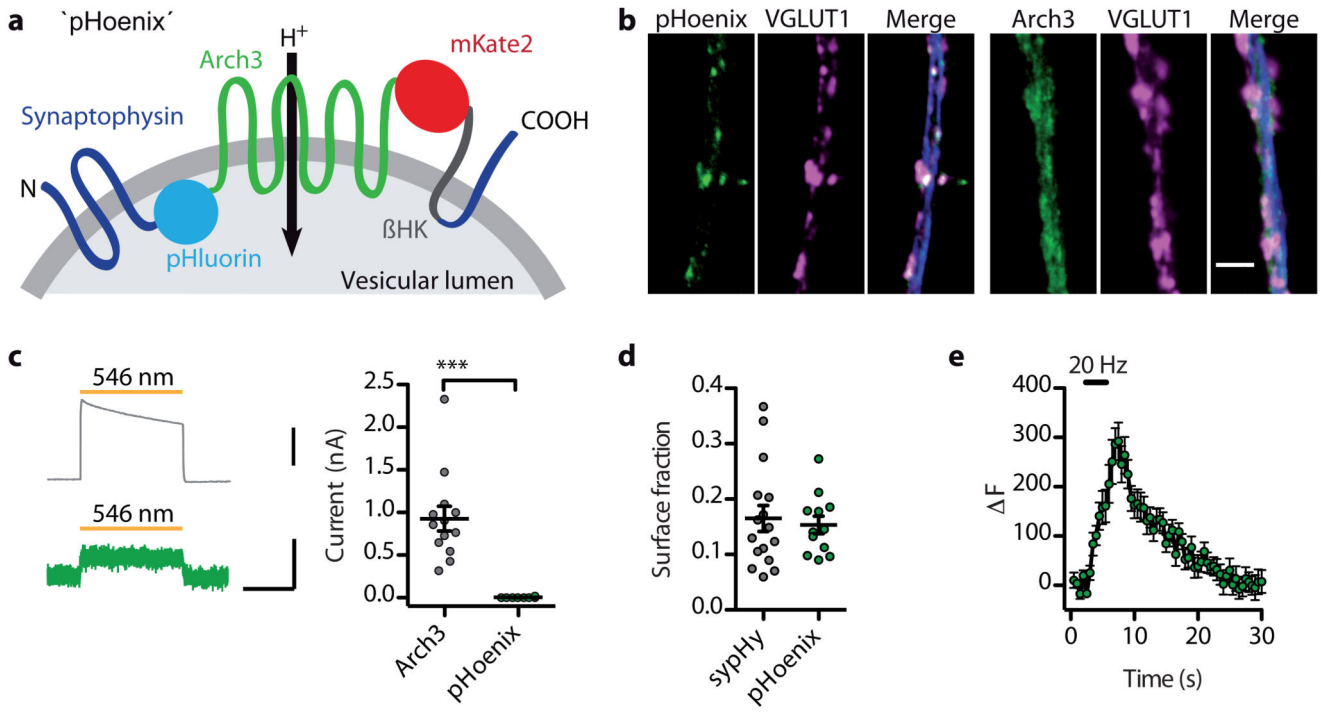

Fig. 1. Design and localization of the light-driven vesicular proton pump pHoenix.

(**a**) Membrane topology of the pHoenix construct. βHK: H^+/K^+ ATPase beta-subunit. (**b**) Confocal images displaying a dendritic segment of a neuron expressing pHoenix or Arch3-eGFP (green), counterstained for the presynaptic marker VGLUT1 (magenta) and the dendritic marker MAP2 (blue). Scale bar, 3 μm. (**c**) Membrane currents evoked by brief light applications in Arch3- (upper trace; scale bar, 500 pA) or pHoenix-expressing neurons (lower trace; scale bars, 500 ms, 50 pA). Arch3-positive cells showed currents of 0.9 ± 0.1 nA ($n = 13$, $N = 2$), while in pHoenix-positive cells light triggered only small currents (3.6 ± 2.1 pA, $n = 8$, $N = 2$; $P = 0.0002$, Mann-Whitney U test, $U = 0$). (**d**) Surface fractions of sypHy and pHoenix at synaptic terminals were 0.17 ± 0.02 for sypHy ($n = 16$) compared to 0.15 ± 0.02 for pHoenix ($n = 12$, $N = 3$; $P = 0.7$, unpaired two-tailed t-test, $t_{26} = 0.378$). (**e**) Exocytosis triggered by 60 APs at 20 Hz increased pHluorin signals due to membrane fusion of pHoenix-containing synaptic vesicles ($n = 11$, $N = 4$).

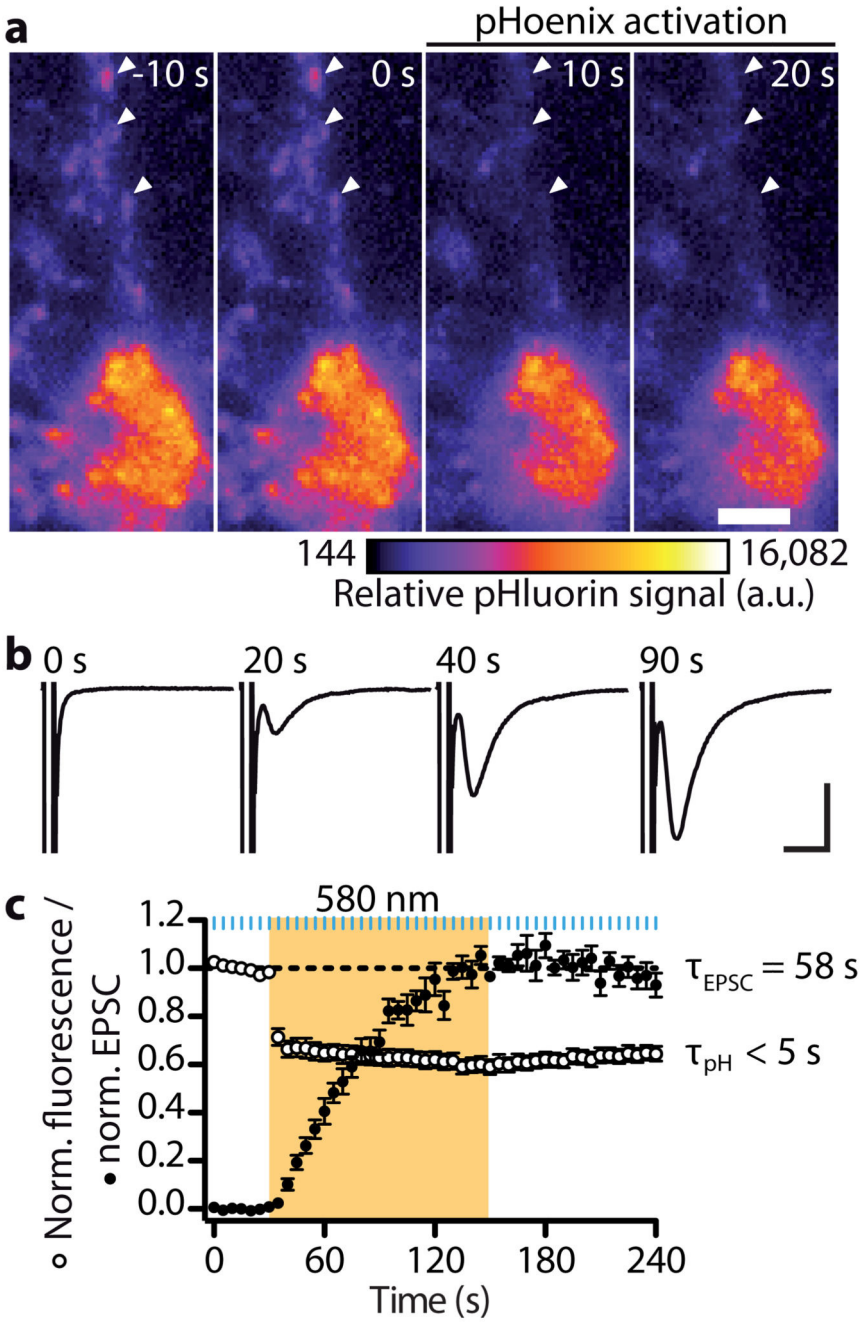

Fig. 2. pHoenix can substitute for V-ATPase function.

(**a**) pHluorin signals of a pHoenix-expressing, Baf-treated neuron acquired before (time point – 10 and 0 s) and during (10 and 20 s) pHoenix activation. Arrowheads indicate synaptic contacts. Scale bar, 10 μm. (**b**) EPSCs recorded from a Baf-treated neuron at indicated time points during pHoenix activation. Scale bars, 5 ms and 1nA. (**c**) Time-plot of normalized pHluorin signals and normalized EPSCs recorded in parallel from Baf-treated, pHoenix-expressing cells ($n = 15$, $N = 2$). Fluorescence of pHluorin molecules was imaged at 0.2 Hz using 100 ms flashes of a 490 nm LED (dotted blue line), just before APs were

triggered. Vesicle acidification by pHoenix and transmitter uptake was induced by interlaced illumination with yellow light.

Europe PMC Funders Author Manuscripts

Europe PMC Funders Author Manuscripts

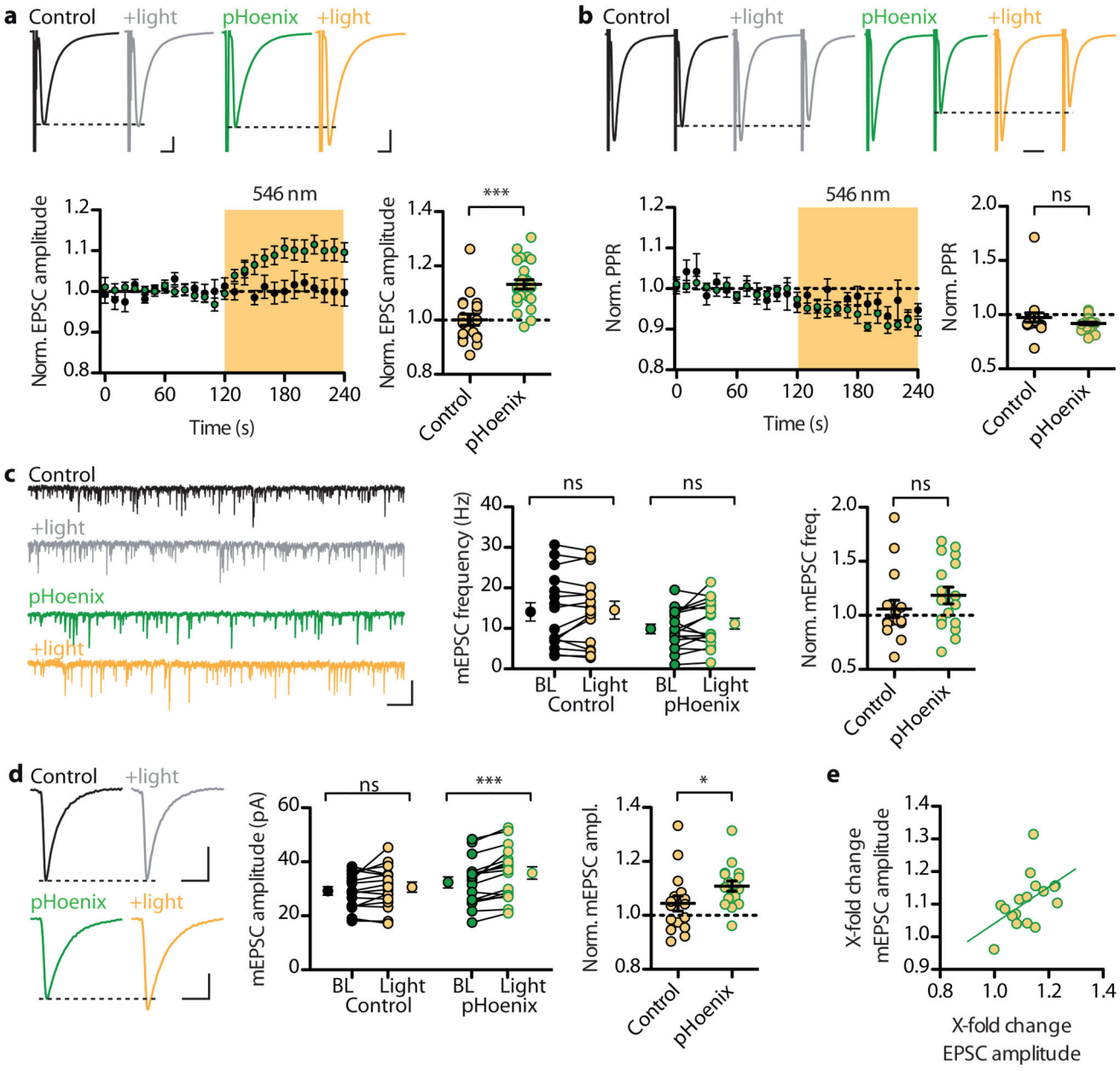

Fig. 3. Activation of pHoenix in untreated neurons increases the quantal size

(**a**) Averages of four EPSCs recorded before and at the end of the 2 min illumination period from a control and a pHoenix-expressing neuron. Scale bars, 5 ms and 2 nA. Illumination had no effect on EPSCs evoked at 0.1 Hz in control neurons (0.1 ± 2%, $n = 19$, $N = 7$), but increased EPSCs in pHoenix expressing neurons by 13 ± 2% ($n = 24$, $N = 7$; $P < 0.0001$, Mann-Whitney U test; $U = 55$). (**b**) Example traces of paired EPSCs evoked at 40 ms inter-stimulus interval. Amplitudes normalized to the 1st EPSC. Scale bar, 10 ms. Paired-pulse ratio changes were not different between the control and pHoenix group ($P = 0.1$, two-tailed Mann-Whitney U test, $U = 159$). (**c**) Spontaneous quantal release events were analyzed from a 1 min period preceding light and the second minute of illumination. Light did not alter the

frequency of mEPSCs (Control cells: baseline (BL): 14.1 ± 2.3 Hz, light: 14.5 ± 2.2 Hz; n = 16, N = 7; P = 0.5, paired two-tailed t-test, t_{15} = 0.701; pHoenix cells: BL = 9.9 ± 1.2 Hz, light: 11.2 ± 1.4 Hz; n = 17, N = 7; P = 0.1, paired two-tailed t-test, t_{16} = 1.809. Scale bar, 200 ms and 50 pA. The mEPSC frequency change in pHoenix expressing cells was not significantly different to control neurons (P = 0.2, Mann-Whitney U test, U = 102). (**d**) mEPSC amplitudes increased significantly in pHoenix expressing neurons (BL: 32.4 ± 2.1 pA, light: 35.9 ± 2.3 pA, n = 17, N = 7; P < 0.0001, paired two-tailed t-test, t_{16} = 5.719), but were not significantly altered in control cells (BL: 29.2 ± 1.6 pA, light: 30.6 ± 1.9 pA; n = 16, N = 7; P = 0.13, paired two-tailed t-test, t_{15} = 1.596). Scale bars, 5 ms, 10 pA. The increase of mEPSC amplitudes in pHoenix-positive neurons was significantly different to controls (P = 0.02, Mann-Whitney U test, U = 72). (**e**) Correlation of the EPSC and mEPSC amplitude increase from pHoenix-expressing neurons. Pearson correlation, two-tailed: P = 0.04, R^2 = 0.25; n = 17, N = 7. There was no correlation between the EPSC increase and the change in mEPSC frequency (Pearson correlation, two-tailed: P = 0.25, R^2 = 0.09; correlation not shown).

Europe PMC Funders Author Manuscripts

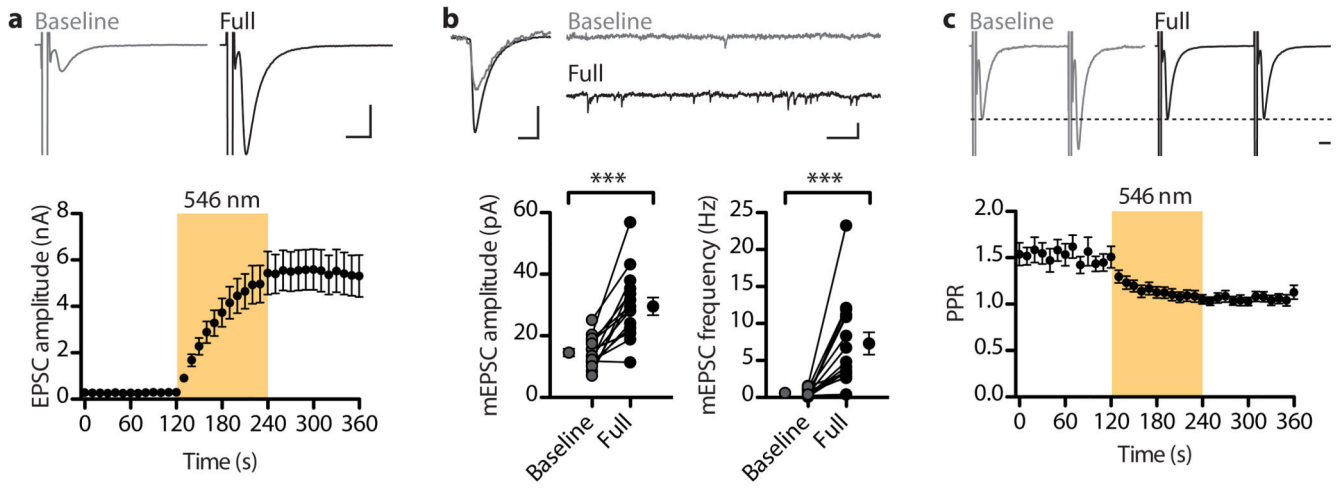

Fig. 4. Neurons with residual glutamate release after Baf-treatment have smaller mEPSCs and a high paired-pulse ratio.

(**a**) Residual EPSC of a neuron incubated for 165 min in Baf (baseline, gray trace), which increased to 400% after pHoenix activation (full, black trace). Scale bars, 5 ms, 0.5 nA. EPSC recovery shown for 20 cells with residual release (0.3 ± 0.1 nA before, 5.5 ± 0.9 nA after illumination, $\tau = 66$ s; $N = 7$). (**b**) Average mEPSCs and example trace of mEPSCs recorded from a neuron before (gray) and after (black) activation of pHoenix. Scale bars, left: 5 ms and 10 pA; right: 100 ms and 50 pA. mEPSC amplitudes increased from 17 ± 2 to 29 ± 3 pA, and mEPSC frequency increased from 0.7 ± 0.2 to 8.1 ± 1.7 Hz ($n = 15$, $N = 7$, amplitudes: $P < 0.0001$, paired two-tailed t-test, $t_{14} = 5.847$; frequency: $P < 0.0001$, Wilcoxon signed-rank test, $W = -120$). (**c**) Paired EPSCs evoked at 40 ms interval during baseline and after pHoenix activation. Amplitudes scaled to first EPSC. Scale bar, 5 ms. Time course of the paired-pulse ratio change from the same cells as in (**a**). PPR decreased from 1.5 ± 0.1 to 1.1 ± 0.1, with $\tau = 23$ s.

Europe PMC Funders Author Manuscripts

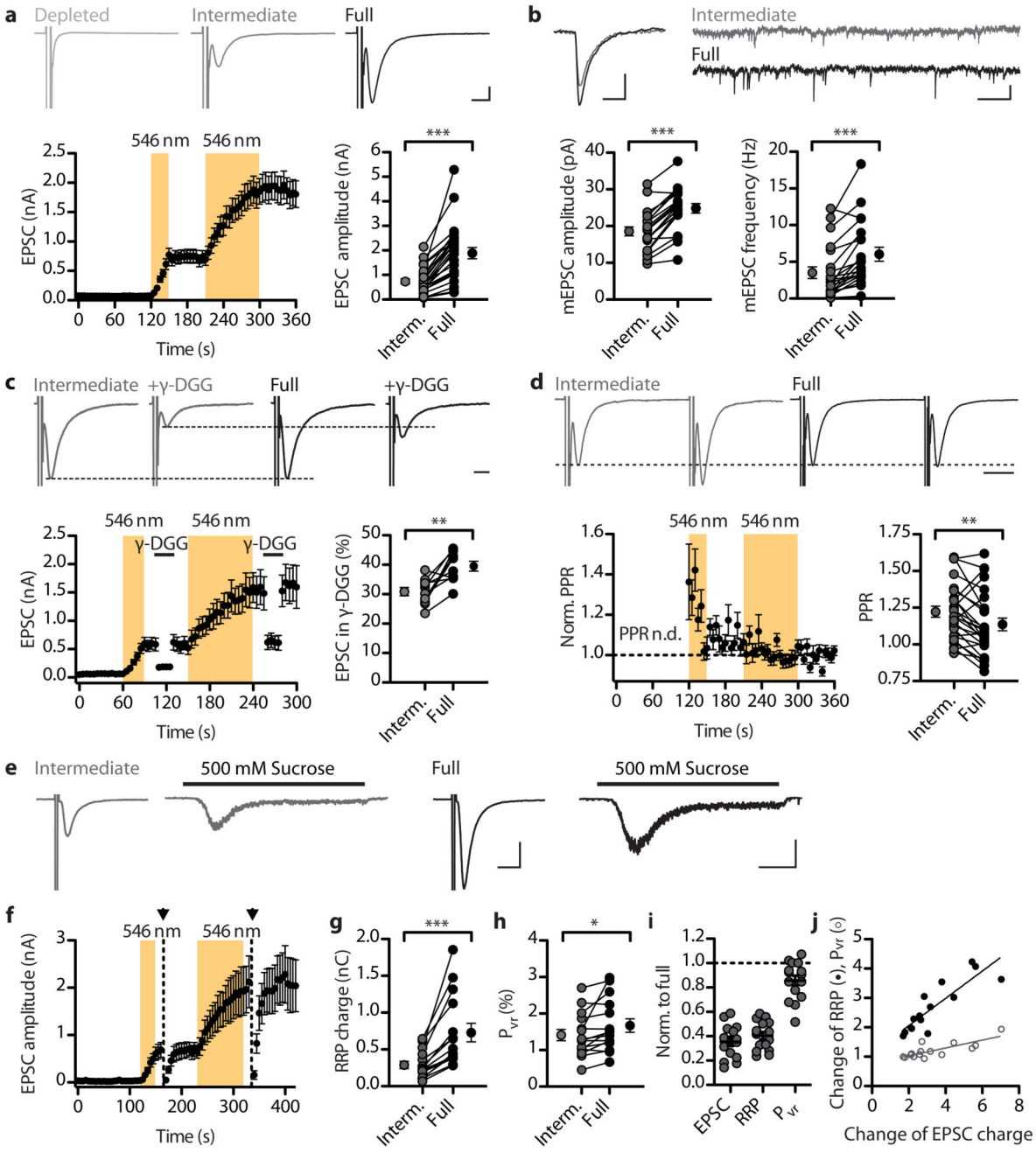

Fig. 5. Partially filled vesicles have a lower release probability.

(**a**) Interval activation of pHoenix allows titration of EPSCs from a depleted to an intermediate and full recovery state. Scale bars, 5 ms, 200 pA. EPSCs recovered during the 30 s of pHoenix activation to 0.7 ± 0.1 nA, remained stable during the intermediate dark phase, and further increased over the following 90 s of illumination to 1.9 ± 0.2 nA ($n = 26$, $N = 6$, $P < 0.0001$, Wilcoxon signed-rank test, W = –351). (**b**) Averages of mEPSCs detected during intermediate (gray) and full recovery condition (black), and typical mEPSC recordings from the same cell. Scale bars, left: 5 ms, 10 pA; right: 200 ms, 25 pA. mEPSC

amplitudes increased from 18.6 ± 1.2 to 24.9 ± 1.3 pA ($n = 21$, $N = 6$; $P < 0.0001$, paired two-tailed t-test, $t_{20} = 9.811$), while the frequency increased from 3.5 ± 0.8 to 6.0 ± 1.0 Hz ($P = 0.0002$, Wilcoxon signed-rank test, W = –217). (**c**) Attenuation of EPSCs by the application of γ-DGG. EPSCs scaled to EPSCs before drug application. Scale bar, 5 ms. γ-DGG application caused an instantaneous drop of EPSC amplitudes ($n = 10$; $N = 2$). The EPSC reduction was stronger during the intermediate fill state compared to the full recovery state ($P = 0.003$, paired two-tailed t-test, $t_9 = 4.155$). (**d**) Average traces of paired EPSCs during intermediate and full recovery condition, normalized to the 1st EPSC. Scale bar, 10 ms. PPR time course during the interval recovery protocol, normalized to the period after the 2nd light interval. During the intermediate recovery state, average PPR was significantly higher compared to the PPR after full recovery (intermediate: 1.22 ± 0.04, full: 1.14 ± 0.04; $n = 26$, $N = 6$; $P = 0.004$, paired two-tailed t-test, $t_{25} = 3.222$). (**e**) Postsynaptic response elicited by application of 500 mM sucrose after intermediate and full recovery of transmission. Averages of EPSCs recorded after the first and the second light interval are shown for comparison. Scale bars, 10 ms, 1 nA for EPSCs; 1 s, 1 nA for sucrose responses (**f**) Hypertonic sucrose solution was applied after the first and second light interval, at time points indicated by arrows. EPSC amplitudes recovered after the depletion of the RRP ($n = 15$, $N = 4$). (**g**) The RRP increases from 290 ± 50 pC to 730 ± 130 pC ($P = 0.0002$, paired two-tailed t-test, $t_{14} = 5.116$). (**h**) The P_{vr} increases from 1.4 ± 0.2% to 1.7 ± 0.2% ($P = 0.02$, paired two-tailed t-test, $t_{14} = 2.665$). (**i**) EPSC charge, RRP and P_{vr} during the intermediate state normalized to the full recovery state. (**j**) The increase of the EPSC from the intermediate to the full recovery state correlates with the increase of the RRP (Pearson correlation, $P < 0.0001$, $R^2 = 0.75$) and the P_{vr} (Spearman correlation, $P = 0.003$).

Europe PMC Funders Author Manuscripts

Europe PMC Funders Author Manuscripts

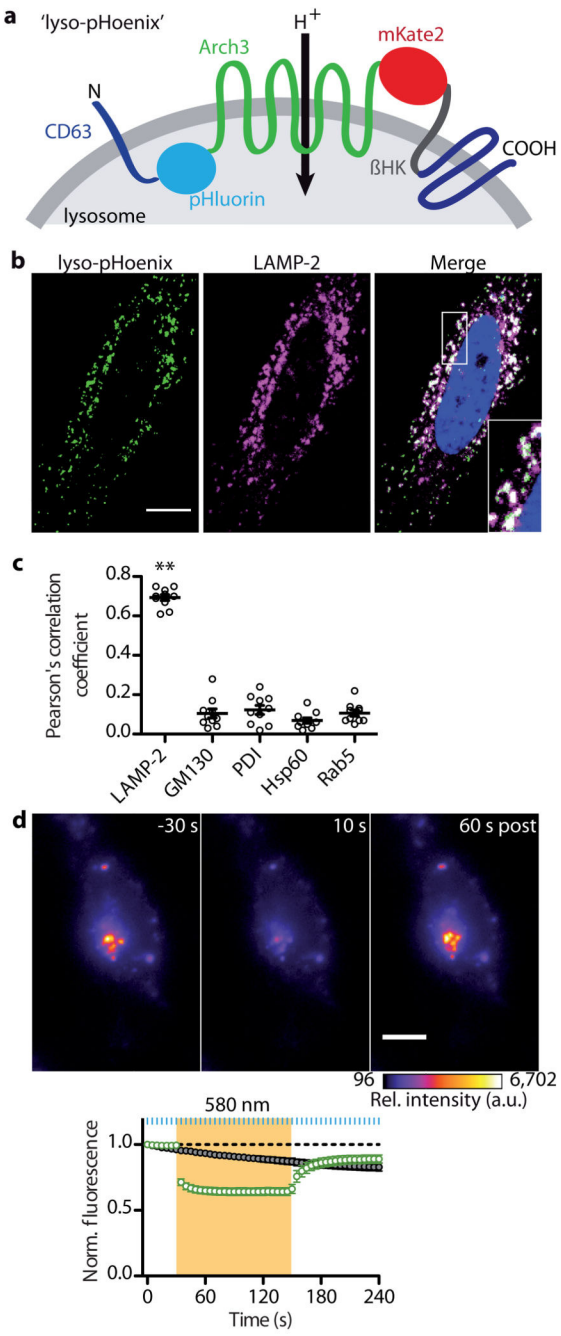

Fig. 6. Optogenetic acidification of lysosomes.

(**a**) Schematic of the lyso-pHoenix construct, with CD63 flanking Arch3, the fluorophores and the βHK transmembrane domain. (**b**) Confocal images of a HeLa cell expressing lyso-pHoenix (green, signal enhanced by anti-GFP antibody), stained for LAMP-2 (magenta), and the nucleus stained with DAPI. Scale bar, 10 μm. (**c**) Quantification of lyso-pHoenix colocalization with different organelle marker proteins ($n = 10$, $N = 2$). Lyso-pHoenix shows a high degree of colocalization with the lysosome marker LAMP-2, but not with markers for the cis-Golgi (GM130), endoplasmic reticulum (PDI), mitochondria (Hsp60) and endosomes

(Rab5). Analyzed by one-way ANOVA, with Tukey's multiple comparison test: $P < 0.001$ for LAMP-2 vs. all other markers, F(4,45) = 203.6. (**d**) Images of a Baf-treated HEK 293 cell acquired before, during and after activation of lyso-pHoenix (averages of two frames). Scale bar, 10 μm. Illumination rapidly decreases pHluorin signals due to lysosomal acidification ($n = 18$, $N = 2$). This effect is not seen in Baf-treated cells expressing CD63-pHluorin ($n = 15$, $N = 2$).

Europe PMC Funders Author Manuscripts